Interaction of Bacteriophage λ Protein Phosphatase with Mn(II): Evidence for the Formation of a $[Mn(II)]_2$ Cluster†

Frank Rusnak,*,‡ Lian Yu,‡ Smilja Todorovic,‡,§ and Pamela Mertz‡

Department of Biochemistry and Molecular Biology and Section of Hematology Research, Mayo Clinic and Foundation, Rochester, Minnesota 55905, and Faculty of Physical Chemistry, University of Belgrade, Belgrade, Yugoslavia

Received November 3, 1998; Revised Manuscript Received March 18, 1999

ABSTRACT: The interaction of bacteriophage λ protein phosphatase with Mn^{2+} was studied using biochemical techniques and electron paramagnetic resonance spectrometry. Reconstitution of bacteriophage λ protein phosphatase in the presence of excess $MnCl_2$ followed by rapid desalting over a gel filtration column resulted in the retention of approximately 1 equiv of Mn^{2+} ion bound to the protein. This was determined by metal analyses and low-temperature EPR spectrometry, the latter of which provided evidence of a mononuclear high-spin Mn^{2+} ion in a ligand environment of oxygen and nitrogen atoms. The Mn^{2+}-reconstituted enzyme exhibited negligible phosphatase activity in the absence of added $MnCl_2$. The EPR spectrum of the mononuclear species disappeared upon the addition of a second equivalent of Mn^{2+} and was replaced by a spectrum attributed to an exchange-coupled $(Mn^{2+})_2$ cluster. EPR spectra of the dinuclear $(Mn^{2+})_2$ cluster were characterized by the presence of multiline features with a hyperfine splitting of 39 G. Temperature-dependent studies indicated that these features arose from an excited state. Titrations of the apoprotein with $MnCl_2$ provided evidence of one Mn^{2+} binding site with a micromolar affinity and at least one additional Mn^{2+} site with a 100-fold lower affinity. The dependence of the phosphatase activity on Mn^{2+} concentration indicates that full enzyme activity probably requires occupation of both Mn^{2+} sites. These results are discussed in the context of divalent metal ion activation of this enzyme and possible roles for Mn^{2+} activation of other serine/threonine protein phosphatases.

All organisms, from bacteria to eukaryotes, utilize reversible phosphorylation of proteins as a primary mechanism for metabolic regulation (*1*−*3*). Protein phosphorylation occurs on serine, threonine, tyrosine, histidine, and aspartic acid, and is catalyzed by protein kinases (*2*, *4*, *5*). Removal of the phosphoryl group is catalyzed by protein phosphatases, and two major groups have been identified, the protein tyrosine phosphatases and the serine/threonine phosphatases (*6*, *7*). The latter have been traditionally classified as type 1 and type 2 serine/threonine protein phosphatases on the basis of their substrate specificity, divalent metal ion dependence, and inhibition by various phosphatase inhibitors (*8*−*11*). Of these enzymes, protein phosphatase 1 (PP1),[1] 2A (PP2A), and calcineurin share approximately 50% sequence identity within their active site domains and are therefore evolutionarily related (*6*, *10*, *12*).

PP1, PP2A, and calcineurin are members of a much larger superfamily of enzymes sharing a common catalytic core. The conserved sequence motif, termed the phosphoesterase motif, consists of the sequence **D**X**H**$(X)_n$G**D**XXD$(X)_m$G**N**-HD/E (*12*−*14*). Enzymes in this superfamily are involved in the hydrolysis of various phosphate esters and include acid and alkaline phosphatases, exonucleases, nucleotidases, diadenosine tetraphosphatases, cyclic nucleotide phosphodiesterases, sphingomyelin phosphodiesterases, the eukaryotic serine/threonine protein phosphatases, and a protein phosphatase from bacteriophage λ which is the subject of this report (*13*, *14*). The X-ray structures of PP1 (*15*, *16*) and calcineurin (*17*, *18*) indicate that the phosphoesterase motif is represented as a β−α−β−α−β secondary element that provides the framework for an active site dinuclear metal cofactor, with the four bold residues highlighted in the above sequence serving as ligands to one metal ion or both metal ions. Similarly, the X-ray structure of kidney bean purple acid phosphatase (*19*, *20*) also indicates a homologous β−α−β−α−β motif accommodating a dinuclear metal cofactor, albeit with a slight variation in the phosphoesterase motif and ligand environment of the metal ions (*11*, *14*).

The high degree of sequence conservation within the phosphoesterase motif in this family of enzymes suggests that other members will share a common active site architecture and catalytic mechanism. Indeed, a protein phosphatase from bacteriophage λ has emerged as a good model for investigating structure−function aspects of the serine/threonine protein phosphatases. Thus, Zhuo et al. (*21*) showed that bacteriophage λ protein phosphatase is a metal requiring enzyme by demonstrating that Mn^{2+} and Ni^{2+} are necessary for activation of the enzyme. Furthermore, Mertz

† This work was supported by Grant GM46865 from the National Institutes of Health.

* To whom correspondence should be addressed: Mayo Clinic and Foundation, 200 First St. S.W., Rochester, MN 55905. Telephone: (507) 284-4743. Fax: (507) 284-8286. E-mail: rusnak@mayo.edu.

‡ Mayo Clinic and Foundation.

§ University of Belgrade.

[1] Abbreviations: DTT, dithiothreitol; EPR, electron paramagnetic resonance; PP1, protein phosphatase 1; PP2A, protein phosphatase 2A; pNPP, *p*-nitrophenyl phosphate; $pNPP^{2-}$, *p*-nitrophenyl phosphate dianion; SD, standard deviation from the mean value.

10.1021/bi982606u CCC: $18.00
Published on Web 05/04/1999

et al. (*22*) demonstrated that recombinant bacteriophage λ protein phosphatase can be reconstituted to contain a dinuclear $Fe^{3+}-Fe^{2+}$ center, analogous to the $Fe^{3+}-Zn^{2+}$ and $Fe^{3+}-Fe^{2+}$ centers of purple acid phosphatase (*23*, *24*), further advancing the hypothesis that enzymes containing the phosphoesterase motif utilize an active site dinuclear metal center.

The identity of the physiological metal ion cofactors for most phosphoesterases is often unknown. As isolated, calcineurin contains a dinuclear $Fe^{3+}-Zn^{2+}$ metal center (*25*, *26*), but the question of whether these represent the physiological metal ions or become incorporated during purification has not been resolved. With that enzyme, the Zn^{2+} ion can be replaced nearly quantitatively with Fe^{2+}, and both the $Fe^{3+}-Zn^{2+}$ and $Fe^{3+}-Fe^{2+}$ forms have comparable enzymatic activity toward either pNPP or a phosphopeptide substrate (*26*, *27*). Nevertheless, calcineurin phosphatase activity can be enhanced by the presence of a divalent metal ion, with Mn^{2+} and Ni^{2+} providing the highest level of activation depending upon the substrate that is used (*25*, *28*−*33*). Similar divalent metal ion activation has been observed for PP1 and PP2A (*34*−*40*). The mechanism for activation is not known, but the addition of a divalent metal such as Mn^{2+} appears to prevent a time-dependent inactivation process that may involve metal substitution (*27*, *29*).

In this study, we have investigated the interaction of recombinant bacteriophage λ protein phosphatase with Mn^{2+}. Mn^{2+} provides an ideal active site probe not only because it is one of the best metal ion activators but also because it is paramagnetic and can be investigated by magnetic resonance techniques. The data for the interaction of bacteriophage λ protein phosphatase with Mn^{2+} as determined by biochemical and EPR spectroscopic techniques are presented in the context of understanding divalent metal ion activation of this phosphatase.

EXPERIMENTAL PROCEDURES

Materials

Dithiothreitol, $MnCl_2$, *p*-nitrophenyl phosphate (pNPP), DEAE-Sepharose CL-6B, and phenyl-Sepharose were purchased from Sigma (St. Louis, MO). YM10 Diaflo ultrafiltration membranes and Centricon microconcentrators were purchased from Amicon, Inc. (Beverly, MA). NAP-25 gel filtration columns were purchased from Pharmacia Biotech (Piscataway, NJ).

Methods

Protein concentrations were measured using the Pierce (Rockford, IL) Coomassie Plus protein assay reagent using bovine serum albumin as a standard. Alternatively, protein concentrations were determined using an ϵ_{281} of 41 700 M^{-1} cm^{-1}. Where noted, errors are represented as standard deviations (SD) from the mean.

Expression and Purification of λ Protein Phosphatase. Expression and purification of bacteriophage λ protein phosphatase were performed as described previously (*21*, *22*, *41*).

Phosphatase Assays. The phosphatase activity was measured at 30 °C in 25 mM Tris-HCl, 50 mM NaCl, 5% glycerol, 1.0 mM DTT (pH 7.5), 10 mM pNPP, 17−50 nM λ protein phosphatase, and, where indicated, various concentrations of $MnCl_2$. The specific activity was measured by following the increase in absorbance at 410 nm with time using an ϵ_{410} of 12 100 (pH 7.5) or 14 400 M^{-1} cm^{-1} (pH 7.8).

For assays of the apoenzyme and Mn^{2+}-reconstituted enzyme, the specific activity of the untreated enzyme (defined as 100% in Table 2) was averaged from three different preparations and obtained by preincubating the enzyme in buffer for 2 min at 30 °C followed by the addition of pNPP to start the reaction. The Mn^{2+}-reconstituted enzyme was obtained by diluting a concentrated solution of the apoenzyme to about 1 mg/mL in 50 mM Tris-HCl, 100 mM NaCl, and 10% glycerol (pH 7.5) in the presence of 1−2 mM $MnCl_2$. This solution was incubated for 5−16 h at 4 °C while it was stirred gently, after which it was concentrated to <2 mL using an Amicon cell equipped with a YM-10 ultrafiltration membrane. The excess $MnCl_2$ was removed by passage over a NAP-25 column into the same buffer without $MnCl_2$, and fractions containing the protein were collected and concentrated to <1 mL using a YM-10 ultrafiltration membrane. The apoenzyme was treated in the same fashion except $MnCl_2$ was excluded from the incubation buffer. Activity measurements of the apoenzyme and Mn^{2+}-reconstituted enzymes were obtained following dilution into 25 mM Tris-HCl, 50 mM NaCl, 1.0 mM DTT, and 5% glycerol (pH 7.5) in the presence or absence of 1 mM $MnCl_2$ and incubated for various times (from 1.5 to 80 min) prior to starting the reaction by addition of pNPP to a final total concentration of 10 mM. The activities noted in Table 2 represent averages ± SD over the time course during which the activity remained constant (from 1.5 to 60 min) from three different preparations of the Mn^{2+}-reconstituted enzyme and two preparations of the apoenzyme.

K_m values for Mn^{2+} binding to λ protein phosphatase were determined at three different concentrations of pNPP (0.1, 1.0, and 10 mM) using 10 different concentrations of $MnCl_2$ from 2 μM to 1 mM, in 100 mM Tris (pH 7.8) and 1−90 nM λ protein phosphatase. The concentration of free Mn^{2+} in the presence of pNPP was calculated from the equilibrium expression using a stability constant of 74 M^{-1} for the Mn−pNPP complex (eq 1) (*42*).

$$K_a = \frac{[Mn-pNPP]}{[Mn^{2+}][pNPP^{2-}]} \quad (1)$$

The effect of protontation of $pNPP^{2-}$ can be ignored since the pK_a for dissociation of the second proton of pNPP is approximately 5.0 (*42*, *43*), indicating that <1% monoanion is present at this pH.

Metal Analysis of λ Protein Phosphatase. Manganese analyses were performed by the Mayo Clinic Metal Laboratory by using a graphite furnace atomic absorption spectrometer (Perkin-Elmer, model 5100).

EPR Analysis of λ Protein Phosphatase Reconstituted with Mn^{2+}. Recombinant λ protein phosphatase at a final concentration of 40 μM (1 mg/mL) in 50−100 mM Tris-HCl (pH 7.5), 5−10% glycerol, 25−100 mM NaCl, and 1 mM $MnCl_2$ was incubated overnight at 4 °C. Following incubation, the protein was concentrated to about 1 mL using an ultrafiltration cell equipped with a YM-10 membrane followed by concentration in a Centricon-10 apparatus. The

sample was then exchanged into the same buffer without $MnCl_2$ by passage over a NAP-25 column (Pharmacia). Buffer exchange using this column was routinely accomplished in less than 5 min. The sample was subsequently concentrated, transferred to a quartz EPR tube, and frozen in liquid nitrogen for EPR analysis.

Low-Temperature EPR of λ Protein Phosphatase Titrated with $MnCl_2$. A sample of λ protein phosphatase in 50 mM Tris-HCl, 10% glycerol, and 100 mM NaCl (pH 7.5) was concentrated to 0.60 mM and frozen in liquid nitrogen, and the EPR spectrum at 3.6 K was recorded. The sample was subsequently thawed and an aliquot of a freshly prepared solution of 1.0 M $MnCl_2$ in water added. Following incubation at room temperature for 10 min, the sample was frozen in liquid nitrogen prior to obtaining another low-temperature EPR spectrum. The titration was continued for up to $\approx$2 equiv of $MnCl_2$ for a total of nine additions of $MnCl_2$, from 80 to 940 μM.

Alternatively, a sample of the apoenzyme was dialyzed at 4 °C for 24 h against 50 mM Tris-HCl, 10% glycerol, and 0.1 M NaCl (pH 7.5) with one change of buffer. Following dialysis, the protein was concentrated to 3 mM and split into equivalent samples. $MnCl_2$ from a 1 M stock solution in water was added to 1 equiv in one sample and 2 equiv in the other. The samples were incubated for 5 min at room temperature and frozen by immersion in liquid nitrogen for EPR analysis.

Titration of λ Protein Phosphatase with $MnCl_2$ As Monitored by Room-Temperature EPR. Standard curves of signal intensity as a function of Mn^{2+} concentration were obtained by plotting the peak-to-trough intensity of one of the six lines of the EPR signal of $Mn(H_2O)_6^{2+}$ at $g = 2.0$ versus the concentration of $MnCl_2$ prepared in 50 mM Tris-HCl, 20% glycerol, and 100 mM NaCl (pH 7.5). The binding of Mn^{2+} to λ protein phosphatase was followed by measuring the signal intensity of the six-line EPR signal of $Mn(H_2O)_6^{2+}$ at room temperature upon addition of $MnCl_2$ to the enzyme. For each EPR sample, a concentrated stock solution of the enzyme was diluted into 50 mM Tris-HCl, 20% glycerol, and 100 mM NaCl (pH 7.5) and a solution of $MnCl_2$ added to the desired final concentration. Following incubation at room temperature for 5 min, the sample was transferred to a quartz EPR flat cell (Wilmad Glass Co., Inc., Buena, NJ) and the EPR spectrum recorded. A new aliquot of protein was used for each Mn^{2+} concentration. The data were fit by least-squares analysis to the following equation (eq 2):

$$\bar{\nu} = \frac{n_1 K_{a1}[Mn^{2+}]}{(1 + K_{a1}[Mn^{2+}])} + \frac{n_2 K_{a2}[Mn^{2+}]}{(1 + K_{a2}[Mn^{2+}])} \qquad (2)$$

In eq 2, $\bar{\nu}$ represents the number of moles of Mn^{2+} bound per mole of protein, n_1 and n_2 represent the number of binding sites with association constants K_{a1} and K_{a2}, respectively, and $[Mn^{2+}]$ represents the concentration of free Mn^{2+}.

Electron Paramagnetic Resonance Spectroscopy. EPR studies were performed on a Bruker ESP300E spectrometer operating at a 9 GHz (X-band) microwave frequency. An Oxford Instruments ESR 900 continuous flow cryostat was used for temperature regulation at low (3.6−100 K) temperatures.

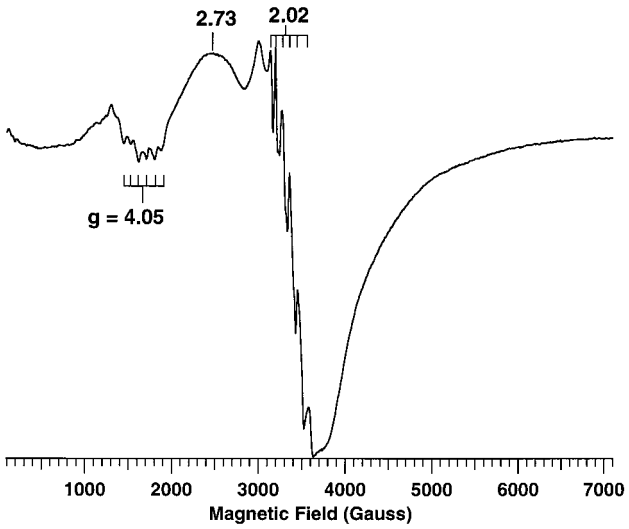

FIGURE 1: Low-temperature EPR spectra of λ protein phosphatase following reconstitution with Mn^{2+}. The spectrum was recorded on a sample of λ protein phosphatase prepared as described in Experimental Procedures by incubating with an excess (1.0 mM) of Mn^{2+} followed by concentration and buffer exchange into 100 mM Tris-HCl (pH 7.5) via passage over a NAP-25 column for removal of excess Mn^{2+}. The sample was further concentrated to 0.9 mM for EPR analysis. The spectrometer conditions were as follows: temperature, 3.9 K; microwave frequency, 9.455 GHz; modulation amplitude and frequency, 5 G at 100 kHz; microwave power, 1.0 mW; and gain, 5×10^4. The hyperfine pattern and g values of selected resonances are indicated.

RESULTS

Reconstitution of λ Protein Phosphatase with $MnCl_2$: Detection of a High-Affinity Mononuclear Mn^{2+} Binding Site. Figure 1 shows the low-temperature EPR spectrum of recombinant bacteriophage λ protein phosphatase following reconstitution with Mn^{2+} (Figure 1). The sample was prepared by incubation of the enzyme in the presence of a 25-fold excess of Mn^{2+} followed by concentration and removal of the excess Mn^{2+} by passage of the sample over a gel filtration column. The EPR spectrum of Figure 1 is highly anisotropic, and many of the features can be attributed to a mononuclear high-spin Mn^{2+} ion. The magnetic spin levels of high-spin Mn^{2+} ($S = {}^5/_2$) can be described by the spin Hamiltonian, **H** (eq 3) (*44*):

$$\mathbf{H} = D(S_z^2 - S^2) + E(S_x^2 - S_y^2) + g_o\beta\vec{\mathbf{H}}\cdot\vec{\mathbf{S}} + A\vec{\mathbf{S}}\cdot\vec{\mathbf{I}} \quad (3)$$

where D and E represent zero-field splitting terms, g_o is the intrinsic g value for Mn^{2+}, β is the Bohr magneton, and A is the hyperfine constant describing the strength of the interaction between the electronic spin and the nuclear spin of ^{55}Mn ($I = {}^5/_2$). In the absence of an applied magnetic field, the zero-field splitting term results in three Kramers doublets with m_s values $\pm{}^1/_2$, $\pm{}^3/_2$, and $\pm{}^5/_2$. The application of an external magnetic field lifts remaining degeneracies according to the Zeeman interaction, while the presence of the nuclear spin of ^{55}Mn yields $2I + 1$ additional m_i levels within each electronic spin state that result in a six-line hyperfine pattern for each of the EPR transitions. Transitions are "allowed" when $\Delta m_s = \pm 1$ and $\Delta m_i = 0$, yielding 30 possible fine structure transitions.

A nearly isotropic resonance centered around $g = 2.0$, corresponding to transitions between $m_s = \pm{}^1/_2$ levels, can

be observed in Figure 1. Six hyperfine lines are evident for this feature and are indicated by the marks above the resonance. The average splitting between hyperfine lines corresponds to an *A* value of approximately 88 G and is consistent with a mononuclear high-spin Mn^{2+} ion bound to the enzyme in a coordination environment of nitrogen and oxygen ligands (*44*). Additional features are clearly evident in the spectrum of Figure 1 such as the peak at $g = 2.73$, a resonance displaying a six-line hyperfine pattern (average splitting of 87 G) centered at $g = 4.05$, and a weak, near zero-field transition at $\mathbf{H} \leq 0.4$ kG ($g \geq 17$, Figure 1). Due to its resonance position and the presence of resolved hyperfine splitting, we attribute the six-line feature at $g = 4.05$ to a "forbidden" $\Delta m_s = \pm 2$ transition, often observed for Mn^{2+} ions that have a relatively large zero-field splitting (*44*−*46*). The other resonances are most likely due to additional outer fine structure transitions (e.g., $m_s = \pm 5/2 \leftrightarrow \pm 3/2$; $m_s = \pm 3/2 \leftrightarrow \pm 1/2$).

Data from manganese analyses of three independent samples of Mn^{2+}-reconstituted λ protein phosphatase samples, including the sample of Figure 1, are listed in Table 1. For these analyses, an average stoichiometry of 0.90 ± 0.1 mol of Mn per mole of protein was obtained. Taken together, the EPR and metal analyses results indicate that approximately one Mn^{2+} ion remains tightly bound to the sample following reconstitution.

EPR Spectra of λ Protein Phosphatase during Mn^{2+} Titration. EPR spectra were also obtained for λ protein phosphatase to which substoichiometric quantities of Mn^{2+} were added stepwise for up to 2 equiv. EPR spectra of λ protein phosphatase following the addition of Mn^{2+} for up to 0.8 equiv are shown in Figure 2. The same resonances observed in Figure 1 such as the six-line features at $g = 4.05$ and 2.02 with an *A* of 87−88 G and the resonances at $g \geq 17$ and $g = 2.7-2.9$ are observed in all spectra in Figure 2 (except that for the apoprotein, top spectrum). The six-line feature at $g = 4.05$ increases in proportion to the Mn^{2+} concentration (see below), a result consistent with the first equivalent of Mn^{2+} binding primarily to a single site. There are minor differences in the spectra of Figure 2 as the Mn^{2+} concentration increases toward 1 equiv. These include a shift of the feature which appears at $g \approx 2.7$ at low Mn^{2+} concentrations to a slightly lower field ($g \approx 2.9$) at higher Mn^{2+} concentrations, and a corresponding increase in its intensity relative to other features in the spectrum. A further difference includes an increase in the intensity near 3.6 kG at higher Mn^{2+} concentrations. At present, we are unable to resolve the spectra well enough to identify the nature of these differences, but they may represent features that can be attributed to a dinuclear $(Mn^{2+})_2$ cluster beginning to form on the enzyme (see below). The fact that each spectrum in Figure 2 is qualitatively similar to the spectrum of Figure 1 indicates that repetitive freeze−thaw cycles during titration do not result in appreciable sample damage.

Table 1: Metal Analysis of Bacteriophage λ Protein Phosphatase following Reconstitution with Mn^{2+} [a]

sample	[protein] (μM)	[Mn^{2+}] (μM)	[Mn^{2+}]/[protein]
1	20 ± 3	19.0 ± 0.2	0.95
2	60 ± 9	49 ± 5	0.82
3	56 ± 8	50.2 ± 0.6	0.89

[a] λ protein phosphatase was incubated with a 25-fold excess of $MnCl_2$ and concentrated, the excess $MnCl_2$ removed via passage over a NAP-25 column, and the sample concentrated for low-temperature EPR. A portion of each EPR sample was diluted into metal free water and analyzed for manganese by atomic absorption spectrophotometry. Protein concentration determinations were performed as described in Experimental Procedures. The values listed for manganese determination represent averages ± the standard deviation from the mean value from replicate analyses. The error in protein concentration determination is estimated to be ±15%.

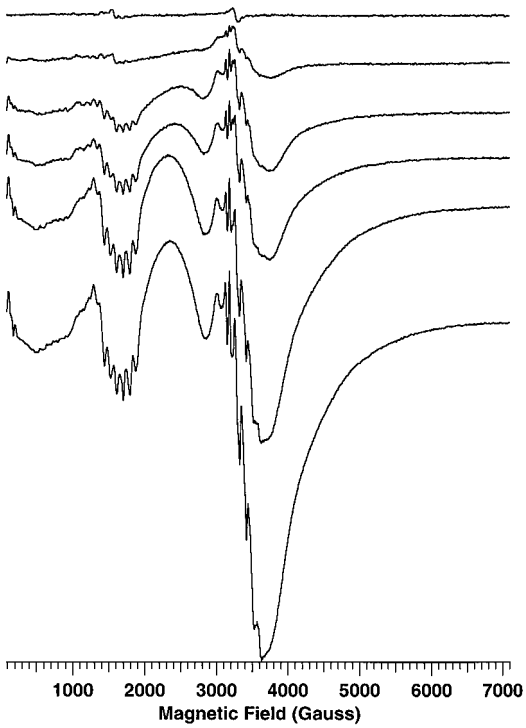

FIGURE 2: EPR spectra of λ protein phosphatase titrated up to 0.8 equiv with Mn^{2+}. The EPR spectra from top to bottom were recorded on a sample of 600 μM λ protein phosphatase in 50 mM Tris-HCl, 10% glycerol, and 100 mM NaCl (pH 7.5) following the addition of $MnCl_2$ to final concentrations of 0, 80, 160, 270, 385, and 490 μM $MnCl_2$. The spectra are plotted for direct comparison of intensity. Spectrometer conditions for all spectra were as follows: temperature, 3.4 K; microwave frequency, 9.45 GHz; modulation amplitude and frequency, 5.2 G at 100 kHz; microwave power, 1.0 mW; and gain, 5×10^4.

Identification of a Second Mn^{2+} Binding Site: Formation of a Spin-Coupled $(Mn^{2+})_2$ Center. Additional aliquots of Mn^{2+} resulted in a decrease in the signal intensity of many of the features noted in Figure 2 as the concentration of Mn^{2+} increased toward 2 equiv (Figure 3). Most notable were decreases in the intensity of the six-line feature at $g = 4.05$ and the low-field resonance ($g \geq 17$). The six-line feature at $g = 4.05$ exhibited a maximum intensity at a Mn^{2+} concentration corresponding to 0.8 equiv (represented by the last spectrum in Figure 2 at a total Mn^{2+} concentration of 490 μM). Further additions of Mn^{2+} resulted in the disappearance of this resonance and the appearance of a spectrum that we attribute to a spin-coupled $(Mn^{2+})_2$ cluster.

If two paramagnetic Mn^{2+} ions are bound in close proximity, their spins will interact via exchange coupling mechanisms. The spin Hamiltonian describing a coupled $(Mn^{2+})_2$ cluster can be written as a sum of zero-field splitting and Zeeman terms for each metal ion (cf. eq 3) as well as an additional Heisenberg exchange coupling term describing the strength of the interaction between paramagnetic centers (eq 4):

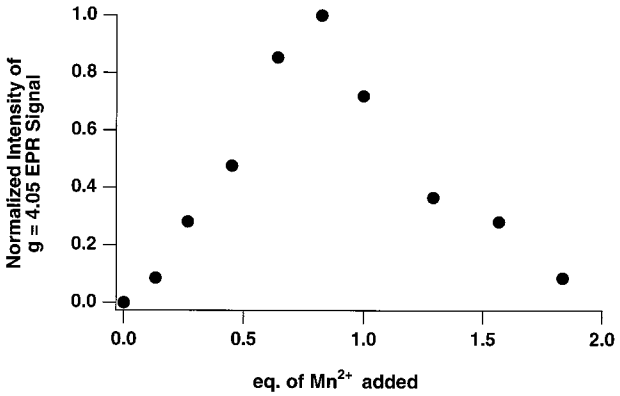

FIGURE 3: Dependence of the intensity of the six-line, $g = 4.05$ resonance, on total Mn^{2+} concentration. A titration of λ protein phosphatase with various concentrations of $MnCl_2$ was performed as described in the legend of Figure 2 and the Experimental Procedures. The intensity (peak-to-trough) of the hyperfine-split resonance in the $g = 4.05$ region was plotted as a function of the number of equivalents of $MnCl_2$ added to the enzyme. The signal was normalized by dividing the intensity of the $g = 4.05$ feature in each sample by the maximum intensity, obtained when $[Mn^{2+}]_{total} = 490\ \mu M$. Spectrometer conditions were the same as described in the legend of Figure 2.

$$\mathbf{H}' = J\vec{\mathbf{S}}_1 \cdot \vec{\mathbf{S}}_2 \qquad (4)$$

In eq 4, S_1 and S_2 represent the spin of each high-spin Mn^{2+} ion ($S_1 = S_2 = {}^5/_2$) and the coupling constant J represents the strength of the exchange interaction. If J is the dominant term in the Hamiltonian, a set of states characterized by the total spin S ($S_1 + S_2$) result, where S can take on integral values from $|S_1 - S_2|$ to $S_1 + S_2$ ($S = 0, 1, ..., 5$ for two high-spin Mn^{2+} ions) separated in energy according to the Landé interval rule (eq 5):

$$E = \frac{J}{2}[S(S+1) - S_1(S_1+1) - S_2(S+1)] \qquad (5)$$

For antiferromagnetic coupling, the ground state is diamagnetic ($S = 0$) and is EPR silent while each excited state ($S = 1, 2, ..., 5$) can give rise to a unique EPR spectrum. Thus, the observed EPR spectra are temperature-dependent and represent a sum of spectra contributed from each spin level weighted according to a Boltzman distribution governed by eq 5 and the temperature of the system (eq 6).

$$n_s(T) = \frac{(2S+1)\exp[-S(S+1)J/kT]}{\sum_i (2S_i+1)\exp[-S(S_i+1)J/kT]} \qquad (6)$$

The 3.7 K EPR spectra of a sample of apoenzyme treated with either 1 or 2 equiv of $MnCl_2$ are shown in Figure 4. The EPR spectrum of λ protein phosphatase in the presence of 1 equiv of Mn^{2+} (Figure 4A) is essentially identical to the spectra in Figures 1 and 2 and represents a mononuclear Mn^{2+} ion bound to the enzyme. The sample of λ protein phosphatase treated with 2 equiv of Mn^{2+} is shown in Figure 4B. In comparing the spectra of panels A and B of Figure 4, we observed several notable differences. First, the six-line feature at $g = 4.05$ in Figure 4B is weaker in intensity by more than 75% relative to this feature in Figure 4A. In addition, the low-field transition at $g \geq 17$ observed in the EPR spectrum of the mononuclear Mn^{2+} site is absent, and

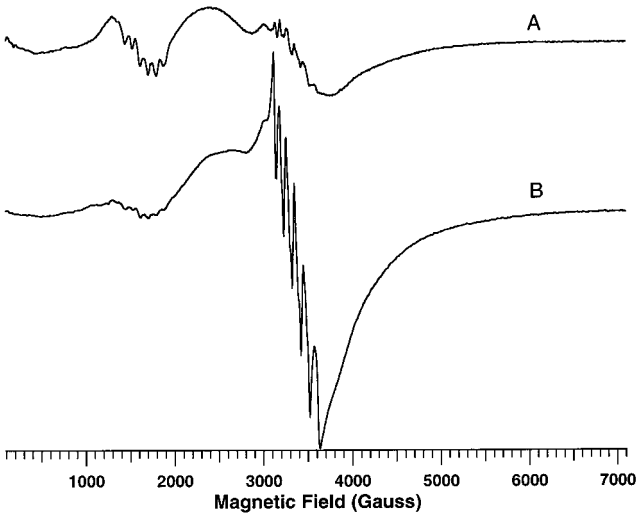

FIGURE 4: Low-temperature EPR spectra of λ protein phosphatase following the addition of either 1 or 2 equiv of Mn^{2+}. Spectrum A is the 3.6 K EPR spectrum of 3.0 mM λ protein phosphatase in 50 mM Tris-HCl, 10% glycerol, and 100 mM NaCl (pH 7.5), following the addition of 3.0 mM $MnCl_2$ (1 equiv). The 3.6 K EPR spectrum (B) was obtained on a sample of λ protein phosphatase following the addition of $MnCl_2$ to 6.0 mM (2 equiv). Spectrometer conditions were as follows: microwave frequency, 9.45 GHz; modulation amplitude and frequency, 2.1 G at 100 kHz; microwave power, 0.25 mW; and gain, 5×10^4.

the feature at $g = 2.7-2.9$ appears to have been replaced by a new feature at $g = 2.7$ which is broad and not resolved. Last, a six-line EPR signal near $g = 2$ from a trace amount of free $Mn(H_2O)_6{}^{2+}$ can be seen in Figure 4B. Despite using high concentrations of protein to minimize the presence of $Mn(H_2O)_6{}^{2+}$ and maximize the binding of Mn^{2+} to the protein, the small amount of $Mn(H_2O)_6{}^{2+}$ dominates the spectrum in the $g = 2$ region (*44*). The EPR spectra of $Mn(H_2O)_6{}^{2+}$ and the residual mononuclear Mn^{2+} site effectively obscure the EPR spectra of any additional components that may be present at 3.7 K.

EPR spectra of the samples treated with either 1 or 2 equiv of Mn^{2+} recorded at 31 K are shown in Figure 5. Several new features appear at this temperature in the sample containing 2 equiv of Mn^{2+} (compare Figure 5B with Figure 4B). These include distinct resonances at 0.49, 2.30, and 2.69 kG ($g = 14.6$, 2.93, and 2.51, respectively), a shoulder at 4.66 kG ($g = 1.45$), and a very broad feature extending from 5.3 to ≥ 6.6 kG (Figure 5B). These features are not observed at low temperatures, and they are not present in the sample containing 1 equiv of Mn^{2+} at either 3.7 or 31 K (Figures 4A and 5A, respectively). A series of spectra recorded from 3.7 to 130 K suggest that these new features are absent in the spectrum at 3.7 K but begin to appear at ≥ 7 K and reach maximum intensity at $\approx 20-30$ K. These results indicate that they arise from a low-lying excited state(s) that becomes populated as the temperature is increased. At least two of the features in the 30 K temperatures exhibit multiline hyperfine patterns. An expansion of the 31 K spectrum of Figure 5B in the region from 0.5 to 3.0 kG is shown in Figure 6. Two 11-line hyperfine patterns, labeled A and C in Figure 6, exhibit an average splitting of 39 G, a value that is approximately half of that expected for a single high-spin Mn^{2+} ion. These characteristics are representative of exchange-coupled Mn^{2+} ions (*44*). The six-line hyperfine pattern with an A of 89 G at $g = 4.05$ representing a residual amount of

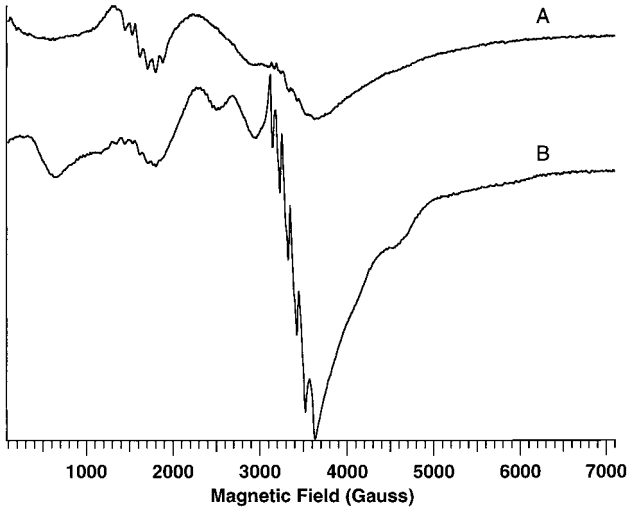

FIGURE 5: EPR spectra of λ protein phosphatase following the addition of 1 or 2 equiv of Mn^{2+} at 31 K. (A) The EPR spectrum of 3.0 mM λ protein phosphatase in the presence of 1 equiv of $MnCl_2$. (B) The EPR spectrum of 3.0 mM λ protein phosphatase in the presence of 2 equiv of $MnCl_2$. The spectra were recorded using the same samples described in the legend of Figure 4. Spectrometer conditions were as follows: microwave frequency, 9.45 GHz; modulation amplitude and frequency, 2.07 G at 100 kHz; microwave power, 20 mW; and receiver gain, 1×10^4.

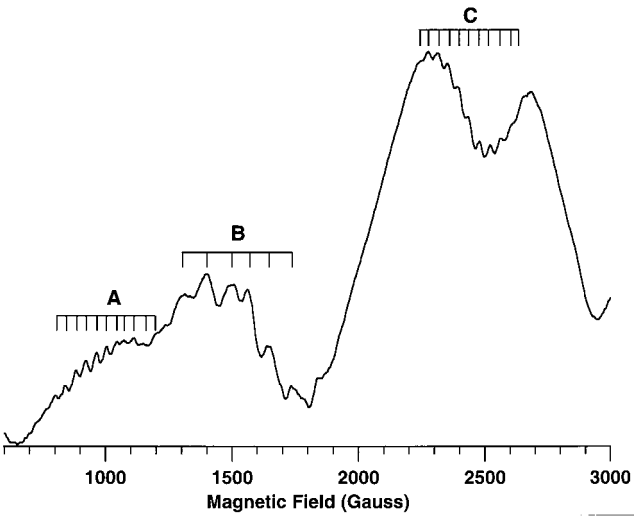

FIGURE 6: Multiline hyperfine pattern of λ protein phosphatase due to the presence of an exchange-coupled $(Mn^{2+})_2$ center. The figure is an expanded-scale version of the 31 K spectrum depicted in Figure 5B. A and C denote the positions of hyperfine-split resonances due to a spin-coupled $(Mn^{2+})_2$ cluster with an average hyperfine splitting of 39 G, while the pattern denoted by B is a residual amount of the six-line, $g = 4.05$ ($A = 87$ G) resonance due to occupancy of the mononuclear site only.

the mononuclear Mn^{2+} ion is highlighted for comparison (pattern B in Figure 6).

Evidence for Two Distinct Mn^{2+} Binding Sites on λ Protein Phosphatase. Further evidence for the presence of two Mn^{2+} binding sites on λ protein phosphatase is provided by titrations of the enzyme with $MnCl_2$ followed by EPR spectrometry at room temperature. In the liquid state, the EPR signal of Mn^{2+} bound to protein is broadened due to zero-field splitting contributions such that it is essentially undetectable at the X-band frequency. For $Mn(H_2O)_6^{2+}$, anisotropy due to zero-field splitting is averaged by rapid tumbling and an isotropic six-line EPR spectrum centered

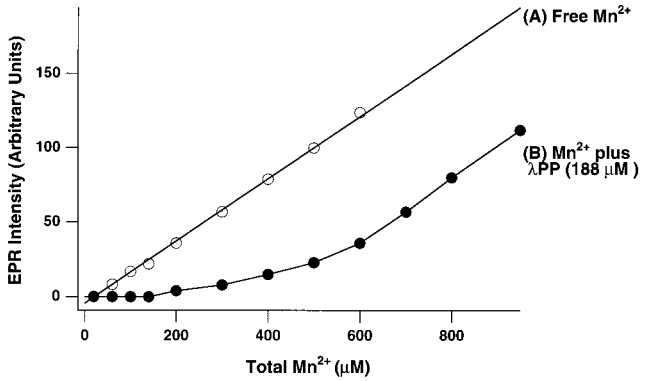

FIGURE 7: Dependence of the intensity of the EPR resonance due to $Mn(H_2O)_6^{2+}$ in the presence and absence of λ protein phosphatase as a function of total $MnCl_2$ concentration. Curve A represents a least-squares fit to the EPR signal intensity of $Mn(H_2O)_6^{2+}$ in 50 mM Tris-HCl, 10% glycerol, and 100 mM NaCl (pH 7.5) as a function of total $MnCl_2$ concentration (○). (B) EPR signal intensity of $Mn(H_2O)_6^{2+}$ (●) as a function of total $MnCl_2$ concentration in the presence of 188 μM λ protein phosphatase in the same buffer used for trace A. Spectrometer conditions were as follows: temperature, 300 K; microwave frequency, 9.438 GHz; modulation amplitude and frequency, 2.0 G at 100 kHz; and microwave power, 8.0 mW.

at $g = 2$ is observed. A standard curve of EPR signal intensity versus $Mn(H_2O)_6^{2+}$ concentration can be obtained from EPR spectra of a series of standard $MnCl_2$ solutions (Figure 7). This standard curve can then be used for determining the concentration of free $Mn(H_2O)_6^{2+}$ in equilibrium with Mn^{2+} bound to λ protein phosphatase following addition of $MnCl_2$ to the sample.

Figure 7 shows the results from a typical experiment in which Mn^{2+} was added to buffer in the absence (Figure 7, curve A) and presence (Figure 7, curve B) of λ protein phosphatase. The standard curve in the absence of enzyme is linear over the range of Mn^{2+} concentrations as expected. In the presence of λ protein phosphatase, however, the addition of up to 1 equiv of Mn^{2+} (190 μM) resulted in a negligible EPR signal from $Mn(H_2O)_6^{2+}$, a result indicating that the first equivalent of Mn^{2+} binds to the enzyme. Further additions of $MnCl_2$ of up to 600 μM resulted in a nonlinear dependence of the intensity of the EPR signal due to free $Mn(H_2O)_6^{2+}$ as a function of total Mn^{2+} concentration, a result which indicates that additional Mn^{2+} ions beyond 1 equiv bind to the enzyme.

A binding isotherm from 1×10^{-6} to 1×10^{-3} M Mn^{2+} was obtained and could be fit to a model assuming two types of noninteracting sites with n Mn^{2+} ions bound per site with dissociation constants K_{d1} and K_{d2} according to eq 2 (Figure 8). Due to the fact that Mn^{2+} binding occurs over a range of Mn^{2+} concentrations that spans 3 orders of magnitude, four sets of experiments with different enzyme concentrations were used to obtain the complete binding isotherm. A least-squares fit to eq 2 for these data indicated one tight Mn^{2+} binding site ($n_1 = 0.71$) with a dissociation constant K_{d1} of 2 ± 1 μM and two weaker Mn^{2+} binding sites ($n_2 = 1.9$) with a K_{d2} of 160 ± 20 μM (Figure 8).

Correlation between Mn^{2+} Binding and Enzyme Activity. The phosphatase activities of the apoenzyme and the Mn^{2+}-reconstituted λ protein phosphatase containing approximately 1 equiv of Mn^{2+} were assayed using pNPP as the substrate as shown in Table 2. The apoenzyme assayed in the absence

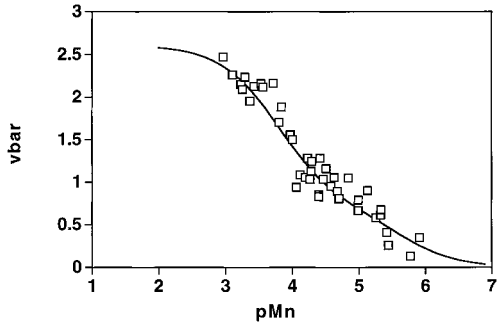

FIGURE 8: Bjerrum plot representing the binding of Mn^{2+} to λ protein phosphatase. The data were collected from four separate titrations of λ protein phosphatase with $MnCl_2$. EPR spectrometer conditions were as follows: temperature, 321 K; and microwave frequency, 9.438 GHz. The modulation amplitude and frequency were 1.0 G at 100 kHz, respectively, and the microwave power was 8.0 mW for samples containing 188 and 200 μM λ protein phosphatase. For samples containing 25 μM λ protein phosphatase, the modulation amplitude was 5.0 G at 100 kHz and the microwave power was 20 mW.

of Mn^{2+} is inactive ($\leq$0.9 μmol of pNPP hydrolyzed min^{-1} mg^{-1}), but the addition of Mn^{2+} to a total concentration of 1 mM results in activation to a specific activity of 260 $\pm$ 70 μmol of pNPP hydrolyzed min^{-1} mg^{-1} (defined as 100% activity for reference, Table 2), verifying the requirement for a divalent metal ion activator (e.g., Mn^{2+} or Ni^{2+}) demonstrated previously by Zhuo et al. (*21*). In comparison, Mn^{2+}-reconstituted bacteriophage λ protein phosphatase had a specific activity of 10.4 $\pm$ 0.8 μmol of pNPP hydrolyzed min^{-1} mg^{-1} when Mn^{2+} was excluded from the assay buffer, 4% of the activity of the fully activated enzyme. The inclusion of Mn^{2+} in the assay buffer increased the specific activity of Mn^{2+}-reconstituted λ protein phosphatase to 70% of the activity of the untreated enzyme. The apoenzyme subjected to the same treatment but without $MnCl_2$ in the incubation buffer was equally as active. The time course for activation was rapid with full activity being achieved in $\leq$5 min.[2] If it is assumed that the tightly bound Mn^{2+} ion does not further dissociate following dilution for activity measurements, these results suggest that a single Mn^{2+} ion bound to the enzyme is not sufficient to activate the enzyme. Additional Mn^{2+} is required to convert the enzyme into the fully active state.

The activation of λ protein phosphatase by Mn^{2+} was explored by assaying the enzyme at total pNPP concentrations of 0.1, 1.0, and 10.0 mM and 10 different total concentrations of $MnCl_2$ from 2 μM to 1 mM. Because pNPP forms a complex with Mn^{2+}, the concentration of free Mn^{2+} available to bind to the enzyme can be calculated from the equilibrium expression in eq 1.

Lineweaver$-$Burk plots for the three concentrations of pNPP were used to estimate the dependence of phosphatase activity on free Mn^{2+} concentration. Replicate measurements at each concentration of pNPP yielded a K_m value of 16 $\pm$ 7 μM for Mn^{2+}, a value in good agreement with the value of 10 μM reported previously for the wild-type enzyme (*41*).

[2] In all but one case, the enzyme activity of the Mn^{2+}-reconstituted enzyme reached 90% of the maximum activity within 2 min following dilution into buffer containing Mn^{2+} and essentially full activity in $\leq$5 min. The activity was stable up to about 60 min but declined slightly after this time. In the one exception, the activity of Mn^{2+}-reconstituted enzyme required a significantly longer time period to reach the maximum (80 min). The reasons for the delayed response for this preparation of enzyme are not understood.

Table 2: Enzyme Activity of the Apoenzyme and Mn^{2+}-Reconstituted Bacteriophage λ Protein Phosphatase in the Presence and Absence of Exogenous Mn^{2+} [a]

sample	% activity (without Mn^{2+})[b]	% activity (with Mn^{2+})[c]
apoenzyme	$\leq$0.3	60 $\pm$ 20
Mn^{2+}-reconstituted enzyme	4.0 $\pm$ 0.3	70 $\pm$ 20

[a] An activity of 260 $\pm$ 70 μmol min^{-1} mg^{-1} (defined as 100% activity) represents the activity of the enzyme in buffer containing Mn^{2+} (see footnote c below) prior to reconstitution. The activities of the apoenzyme or the Mn^{2+}-reconstituted enzyme represent the activities after reconstitution in the presence or absence of Mn^{2+} as described in Experimental Procedures. [b] The assay buffer contained 25 mM Tris-HCl, 50 mM NaCl, 5% glycerol (pH 7.5), 1.0 mM DTT, 10 mM pNPP, and 17$-$50 nM λ protein phosphatase as described in Experimental Procedures. No other source of Mn^{2+} was provided other than that bound to the enzyme prior to dilution into assay buffer. [c] The assay buffer was the same as in footnote b with 1 mM $MnCl_2$.

DISCUSSION

In this study, bacteriophage λ protein phosphatase was reconstituted with Mn^{2+} to understand how this divalent metal ion interacts with the enzyme to activate it for phosphate ester hydrolysis. Incubation of the enzyme in the presence of 1 mM $MnCl_2$, followed by a rapid desalting step over a NAP-25 gel filtration column, resulted in recovery of the enzyme containing approximately 1 equiv of Mn. EPR spectrometry revealed spectra dominated by a single Mn^{2+} ion bound in a coordination environment of oxygen and/or nitrogen ligands, ligands which are predicted by analogy with other enzymes containing the phosphoesterase motif (*14*, *21*). The EPR spectra of this Mn^{2+} ion are quite similar to EPR spectra previously reported for the manganese dioxygenase from *Arthrobacter globiformis* in the presence of 3,4-dihydroxyphenylacetic acid (*47*), and the spectra of Mn^{2+} in ternary complexes of pyruvate kinase with pyruvate or phosphoenolpyruvate (*48*). The X-band EPR spectra of Mn^{2+} ions bound to these enzymes are highly anisotropic and characterized by large zero-field splittings, the result of asymmetry in the ligand environment. The manganese dioxygenase contains a Mn^{2+} binding site consisting of two histidines, a glutamate, and probably either one or two phenolate oxygens from the substrate (*47*, *49*), while an X-ray structure of the pyruvate complex of pyruvate kinase shows a Mn^{2+} ion coordinated by two carboxylates from the protein, the carboxylate and carbonyl group of pyruvate, and possibly two water molecules (*50*). A similar asymmetric Mn^{2+} coordination environment is expected for Mn-reconstituted λ protein phosphatase.

Somewhat unexpected was the absence of a second bound Mn^{2+} ion following reconstitution since the phosphoesterase motif is predicted to accommodate two closely spaced metal ions as a dinuclear metal unit. Indeed, the formation of a spin-coupled $Fe^{3+}-Fe^{2+}$ cluster has been demonstrated in bacteriophage λ protein phosphatase (*22*), indicating that two intimate metal binding sites exist for this protein. Binding of the second Mn^{2+} ion could only be detected when the concentration of free Mn^{2+} exceeded $\approx$100 μM (or 1 equiv for concentrated solutions of the enzyme), implying a much weaker affinity for the second Mn^{2+} ion. λ protein phos-

phatase is thus capable of binding two Mn^{2+} ions, one with high affinity, and a second with much lower affinity that readily dissociates from the enzyme. This was confirmed by Mn^{2+} titrations of the apoenzyme which revealed one binding site ($n_1 = 0.71$) with a micromolar dissociation constant and is attributed to the Mn^{2+} ion that remains tightly associated with the enzyme after desalting. These titrations also indicated at least one additional Mn^{2+} binding site with an approximately 100-fold lower affinity exists. The presence of two divalent metal ion binding sites with disparate affinities has been observed in a number of enzymes such as the Co^{2+}-dependent prolidase from the archeon *Pyrococcus furiosus* (*51*). This enzyme is a member of a separate superfamily of metallohydrolases which utilize dinuclear metal centers as active site cofactors. Other examples include enolase and *S*-adenosylmethionine synthase, both dinuclear metal-containing enzymes which bind one divalent metal ion with high affinity and a second metal with weaker affinity whose binding is facilitated by the presence of the substrate (*52*−*54*).

Although the binding isotherm was best fit by modeling two low-affinity Mn^{2+} ions ($n_2 = 1.9$), the existence of a third divalent metal ion binding site is tenuous. The possibility of three divalent metal ions binding to λ protein phosphatase, in analogy to *Escherichia coli* alkaline phosphatase which binds two Zn^{2+} ions and one Mg^{2+} ion (*55*), is not supported by X-ray structures of other members of this family of enzymes such as purple acid phosphatase, PP1, and calcineurin. Since the highest experimental stoichiometry obtained was 2.4 and exceeded 2 equiv only when the concentration of free Mn^{2+} was ≥ 300 μM (Figure 8), a more likely situation is that nonspecific Mn^{2+} binding is occurring at these high concentrations as has been observed, for example, with Mn^{2+} binding to the $(Zn)_2Mg$ form of *E. coli* alkaline phosphatase (*56*).

Low-temperature EPR spectroscopy indicated that the second Mn^{2+} ion binds close to the first to form a spin-coupled $(Mn^{2+})_2$ cluster. Thus, EPR spectra showed multiline features with an *A* of 39 G which were absent at the lowest temperatures but appeared at ≥ 7 K and exhibited maximum intensity at $\approx$20−30 K. These features are characteristic of exchange-coupled $(Mn^{2+})_2$ centers (*44*) such as those found in enolase (*57*, *58*), *S*-adenosylmethionine synthase (*54*), manganese catalases (*59*−*62*), and rat liver arginase (*63*). The presence of additional paramagnetic components, in particular, residual amounts of the mononuclear Mn^{2+} component and a trace of $Mn(H_2O)_6^{2+}$, effectively obscures the EPR spectra of this coupled $(Mn^{2+})_2$ species for temperatures of $\leq$20 K, making it difficult to follow its temperature dependence with accuracy. Nevertheless, we have attempted simulations of the temperature dependence of several features noted in Figure 5B and found that we could obtain reasonable fits to an $S = 2$ state with a coupling constant (*J*) of about 1−3 cm^{-1} for the features at 0.3, 2.3, and 2.7 kG. The strength of the exchange interaction is a function of the distance between metal ions and the type of ligand bridging the two metal ions (if present). The *J* value estimated for λ protein phosphatase is significantly lower than *J* values observed for manganese catalases but similar to values obtained for rat liver arginase, an analogous metallohydrolase which converts L-arginine to L-ornithine and urea (*61*, *64*). For arginase, the weak coupling was compared to *J* values measured for model $(Mn^{2+})_2$ compounds and used to infer the presence of a μ-H_2O ligand bridging the two Mn^{2+} ions rather than a μ-OH (*64*). Further experiments are in progress to confirm the strength of the exchange interaction and determine the ligand environment in this enzyme for comparison with other metallohydrolases which utilize a dinuclear $(Mn^{2+})_2$ center.

The relationship of enzymatic activity to Mn^{2+} concentration can be estimated by measuring the K_m for Mn^{2+}. In the presence of three different concentrations of pNPP, the K_m for Mn^{2+} was determined to be 16 μM, a value 10-fold lower than the dissociation constant measured for binding of the second Mn^{2+} ion to the enzyme. This result alone could be taken to indicate that the enzyme is active when only one Mn^{2+} ion is bound to the enzyme since this value is only slightly higher than the value estimated for the dissociation constant of the first Mn^{2+} ion that binds to the enzyme in the absence of substrate. Results from Table 2, however, indicate that the Mn^{2+}-reconstituted enzyme has only low activity unless additional Mn^{2+} is added to the assay buffer, a result which suggests that the enzyme requires more than one Mn^{2+} ion for full activity. However, these assessments of Mn^{2+} activation are complicated by the fact that, in addition to binding to the enzyme in the absence of substrate (Figure 8), Mn^{2+} can also bind to substrate pNPP in an independent equilibrium governed by eq 1. It is thus possible that the enzyme binds one Mn^{2+} ion tightly but the second one enters as a complex with substrate; i.e., the Mn−pNPP complex may be the true substrate for the enzyme. Further biochemical and kinetic experiments are necessary to determine the order of metal and substrate binding and the mechanism of the reaction.

We have investigated the binding of Mn^{2+} to bacteriophage λ protein phosphatase to provide insight into the mechanism of divalent metal ion activation. These studies may also provide a framework for understanding the mechanism of divalent metal ion activation of the serine/threonine protein phosphatases calcineurin, PP1, and PP2A. Calcineurin has been shown to be activated by Mn^{2+} and Ni^{2+} (*25*, *28*−*33*). Interestingly, neither Mn nor Ni could be detected in samples of calcineurin following purification (*25*) or rapid immunoprecipitation (*65*), indicating that these are not likely to be native metal ions. Rather, Fe and Zn were found to be tightly associated with the purified enzyme as a dinuclear Fe^{3+}−Zn^{2+} active site cofactor (*17*, *18*, *25*, *26*), analogous to the Fe^{3+}−Zn^{2+} dinuclear site in the purple acid phosphatase from kidney bean (*19*, *66*). Similar divalent metal ion activation has been noted for PP1 and PP2A. Thus, PP2A can be activated by Co^{2+} or Mn^{2+}, and the enzyme that had lost the activity can be reactivated by the same divalent cations (*37*, *38*). PP1 undergoes analogous activation, with Mn^{2+} bringing about the highest level of activity (*34*−*36*, *39*, *40*).

The mechanism of divalent metal ion activation of the serine/threonine protein phosphatases may involve substitution of one or both of the endogenous metal ions present in the native enzyme. Thus, Zn^{2+}, Ni^{2+}, Cu^{2+}, Hg^{2+}, Mn^{2+}, and Co^{2+} have been shown to substitute for the Fe^{2+} site of the Fe^{3+}−Fe^{2+} dinuclear cluster of porcine uteroferrin or beef spleen purple acid phosphatase (*67*−*72*). Similarly, Fe^{2+} can replace the Zn^{2+} ion of the Fe^{3+}−Zn^{2+} center of kidney bean purple acid phosphatase (*66*, *73*) or bovine brain calcineurin (*26*), yielding a spin-coupled Fe^{3+}−Fe^{2+} cluster. Recombi-

nant PP1 used for X-ray studies contained 0.92 equiv of Mn and 0.45 equiv of Fe following crystallization in Mn^{2+}-containing buffers, leading Barford and colleagues to propose an Fe−Mn dinuclear metal center (*16*) and indicating that at least one of the sites of the dinuclear metal center may accommodate a Mn^{2+} ion. Interestingly, prolonged incubation of calcineurin with $^{63}Ni^{2+}$ or $^{54}Mn^{2+}$ leads to the association of up to 2 equiv of these metal ions, suggesting that Ni^{2+} and Mn^{2+} may be able to displace not just one but possibly both of the endogenous (Fe and/or Zn) ions. Recently, Merkx and Averill (*74*) were successful in replacing the Fe^{3+} ion with Ga^{3+} to generate $Ga^{3+}-Fe^{2+}$ and $Ga^{3+}-Zn^{2+}$ forms of bovine spleen purple acid phosphatase, indicating that it is possible to bring about selective substitution of both metal ions.

It is thus reasonable to hypothesize that divalent metal ion activation of calcineurin, PP1, and PP2A may involve substitution of one of the intrinsic metal ions of these enzymes. Continued investigation into the mechanism of divalent metal ion activation of calcineurin, PP1, and PP2A will require careful analytical and spectroscopic analyses to resolve the issue of whether these enzymes have a weakly bound metal ion which can be easily replaced by exogenous divalent metal ions. At least in the case of bacteriophage λ protein phosphatase, we have shown that activation by Mn^{2+} likely requires the assembly of a dinuclear $(Mn^{2+})_2$ site. The presence of two metal sites with different affinities makes it possible to produce mixed metal clusters and allows for the possibility of exploring the roles of individual metal ions of the dinuclear metal center.

ACKNOWLEDGMENT

We thank Mr. Robert Sikkink for technical assistance in preparing the enzyme used in this study.

SUPPORTING INFORMATION AVAILABLE

Three graphs showing the temperature dependence of selected EPR resonances of λ protein phosphatase containing 2 equiv of Mn^{2+} together with theoretical fits to eq 6. This material is available free of charge via the Internet at http://pubs.acs.org.

REFERENCES

1. Hunter, T. (1995) *Cell 80*, 225−236.
2. Kennelly, P. J., and Potts, M. (1996) *J. Bacteriol. 178*, 4759−4764.
3. Smith, S. C., Kennelly, P. J., and Potts, M. (1997) *J. Bacteriol. 179*, 2418−2420.
4. Hunter, T., and Cooper, J. A. (1985) *Annu. Rev. Biochem. 54*, 897−930.
5. Edelman, A. M., Blumenthal, D. K., and Krebs, E. G. (1987) *Annu. Rev. Biochem. 56*, 567−613.
6. Shenolikar, S., and Nairn, A. C. (1991) *Adv. Second Messenger Phosphoprotein Res. 23*, 3−121.
7. Charbonneau, H., and Tonks, N. K. (1992) *Annu. Rev. Cell Biol. 8*, 463−493.
8. Ingebritsen, T. S., and Cohen, P. (1983) *Science 221*, 331−338.
9. Cohen, P. (1989) *Annu. Rev. Biochem. 58*, 453−508.
10. Cohen, P., and Cohen, P. T. W. (1989) *J. Biol. Chem. 264*, 21435−21438.
11. Rusnak, F., Yu, L., and Mertz, P. (1996) *J. Biol. Inorg. Chem. 1*, 388−396.
12. Barton, G. J., Cohen, P. T. W., and Barford, D. (1994) *Eur. J. Biochem. 220*, 225−237.
13. Koonin, E. V. (1994) *Protein Sci. 3*, 356−358.
14. Lohse, D. L., Denu, J. M., and Dixon, J. E. (1995) *Structure 3*, 987−990.
15. Goldberg, J., Huang, H.-B., Kwon, Y.-G., Greengard, P., Nairn, A. C., and Kuriyan, J. (1995) *Nature 376*, 745−753.
16. Egloff, M.-P., Cohen, P. T. W., Reinemer, P., and Barford, D. (1995) *J. Mol. Biol. 254*, 942−959.
17. Griffith, J. P., Kim, J. L., Kim, E. E., Sintchak, M. D., Thomson, J. A., Fitzgibbon, M. J., Fleming, M. A., Caron, P. R., Hsiao, K., and Navia, M. A. (1995) *Cell 82*, 507−522.
18. Kissinger, C. R., Parge, H. E., Knighton, D. R., Lewis, C. T., Pelletier, L. A., Tempczyk, A., Kalish, V. J., Tucker, K. D., Showalter, R. E., Moomaw, E. W., Gastinel, L. N., Habuka, N., Chen, X., Maldonado, F., Barker, J. E., Bacquet, R., and Villafranca, J. E. (1995) *Nature 378*, 641−644.
19. Sträter, N., Klabunde, T., Tucker, P., Witzel, H., and Krebs, B. (1995) *Science 268*, 1489−1492.
20. Klabunde, T., Sträter, N., Frölich, R., Witzel, H., and Krebs, B. (1996) *J. Mol. Biol. 259*, 737−748.
21. Zhuo, S., Clemens, J. C., Hakes, D. J., Barford, D., and Dixon, J. E. (1993) *J. Biol. Chem. 268*, 17754−17761.
22. Mertz, P., Yu, L., Sikkink, R., and Rusnak, F. (1997) *J. Biol. Chem. 272*, 21296−21302.
23. Kurtz, D. M., Jr. (1990) *Chem. Rev. 90*, 585−606.
24. Vincent, J. B., Olivier-Lilley, G. L., and Averill, B. A. (1990) *Chem. Rev. 90*, 1447−1467.
25. King, M. M., and Huang, C. Y. (1984) *J. Biol. Chem. 259*, 8847−8856.
26. Yu, L., Haddy, A., and Rusnak, F. (1995) *J. Am. Chem. Soc. 117*, 10147−10148.
27. Yu, L., Golbeck, J., Yao, J., and Rusnak, F. (1997) *Biochemistry 36*, 10727−10734.
28. King, M. M., and Huang, C. Y. (1983) *Biochem. Biophys. Res. Commun. 114*, 955−961.
29. Pallen, C. J., and Wang, J. H. (1983) *J. Biol. Chem. 258*, 8550−8553.
30. Pallen, C. J., and Wang, J. H. (1984) *J. Biol. Chem. 259*, 6134−6141.
31. Gupta, R. C., Khandelwal, R. L., and Sulakhe, P. V. (1984) *FEBS Lett. 169*, 251−255.
32. Li, H.-C. (1984) *J. Biol. Chem. 259*, 8801−8807.
33. Wolff, D. J., and Sved, D. W. (1985) *J. Biol. Chem. 260*, 4195−4202.
34. Berndt, N., and Cohen, P. T. W. (1990) *Eur. J. Biochem. 190*, 291−297.
35. Zhang, Z., Bai, G., Deans-Zirattu, S., Browner, M. F., and Lee, E. Y. C. (1992) *J. Biol. Chem. 267*, 1484−1490.
36. Alessi, D. R., Street, A. J., Cohen, P., and Cohen, P. T. W. (1993) *Eur. J. Biochem. 213*, 1055−1066.
37. Chu, Y., Wilson, S. E., and Schlender, K. K. (1994) *Biochim. Biophys. Acta 1208*, 45−54.
38. Cai, L., Chu, Y., Wilson, S. E., and Schlender, K. K. (1995) *Biochem. Biophys. Res. Commun. 208*, 274−279.
39. Chu, Y., Lee, E. Y. C., and Schlender, K. K. (1996) *J. Biol. Chem. 271*, 2574−2577.
40. Endo, S., Connor, J. H., Forney, B., Zhang, L., Ingebritsen, T. S., Lee, E. Y. C., and Shenolikar, S. (1997) *Biochemistry 36*, 6986−6992.
41. Zhuo, S., Clemens, J. C., Stone, R. L., and Dixon, J. E. (1994) *J. Biol. Chem. 269*, 26234−26238.
42. Massoud, S. S., and Sigel, H. (1988) *Inorg. Chem. 27*, 1447−1453.
43. Bourne, N., and Williams, A. (1984) *J. Org. Chem. 49*, 1200−1204.
44. Reed, G. H., and Markham, G. D. (1984) *Biol. Magn. Reson. 6*, 73−142.
45. Griscom, D. L., and Griscom, R. E. (1967) *J. Chem. Phys. 47*, 2711−2722.
46. Schreurs, J. W. H. (1978) *J. Chem. Phys. 69*, 2151−2156.
47. Whiting, A. K., Boldt, Y. R., Hendrich, M. P., Wackett, L. P., and Que, L., Jr. (1996) *Biochemistry 35*, 160−170.

48. Reed, G. H., and Cohn, M. (1973) *J. Biol. Chem. 248*, 6436−6442.
49. Boldt, Y. R., Whiting, A. K., Wagner, M. L., Sadowsky, M. J., Que, L., Jr., and Wackett, L. P. (1997) *Biochemistry 36*, 2147−2153.
50. Larsen, T. M., Laughlin, L. T., Holden, H. M., Rayment, I., and Reed, G. H. (1994) *Biochemistry 33*, 6301−6309.
51. Ghosh, M., Grunden, A. M., Dunn, D. M., Weiss, R., and Adams, M. W. W. (1998) *J. Bacteriol. 180*, 4781−4789.
52. Faller, L. D., Baroudy, B. M., Johnson, A. M., and Ewall, R. X. (1977) *Biochemistry 16*, 3864−3869.
53. Reed, G. H., Poyner, R. R., Larsen, T. M., Wedekind, J. E., and Rayment, I. (1996) *Curr. Opin. Struct. Biol. 6*, 736−743.
54. Markham, G. D. (1981) *J. Biol. Chem. 256*, 1903−1909.
55. Coleman, J. E. (1992) *Annu. Rev. Biophys. Biomol. Struct. 21*, 441−483.
56. Schulz, C., Bertini, I., Viezzoli, M. S., Brown, R. D., III, Koenig, S. H., and Coleman, J. E. (1989) *Inorg. Chem. 28*, 1490−1496.
57. Chien, J. C. W., and Westhead, E. W. (1971) *Biochemistry 10*, 3198−3203.
58. Poyner, R. R., and Reed, G. H. (1992) *Biochemistry 31*, 7166−7173.
59. Fronko, R. M., Penner-Hahn, J. E., and Bender, C. J. (1988) *J. Am. Chem. Soc. 110*, 7554−7555.
60. Khangulov, S. V., Barynin, V. V., Voevodskaya, N. V., and Brebenko, A. I. (1990) *Biochim. Biophys. Acta 1020*, 305−310.
61. Khangulov, S. V., Pessiki, P. J., Barynin, V. V., Ash, D. E., and Dismukes, G. C. (1995) *Biochemistry 34*, 2015−2025.
62. Meier, A. E., Whittaker, M. M., and Whittaker, J. W. (1996) *Biochemistry 35*, 348−360.
63. Reczkowski, R. S., and Ash, D. E. (1992) *J. Am. Chem. Soc. 114*, 10992−10994.
64. Khangulov, S. V., Sossong, T. M., Jr., Ash, D. E., and Dismukes, G. C. (1998) *Biochemistry 37*, 8539−8550.
65. Rao, J., and Wang, J. H. (1989) *J. Biol. Chem. 264*, 1058−1061.
66. Beck, J. L., de Jersey, J., Zerner, B., Hendrich, M. P., and Debrunner, P. G. (1988) *J. Am. Chem. Soc. 110*, 3317−3318.
67. Keough, D. T., Dionysius, D. A., de Jersey, J., and Zerner, B. (1980) *Biochem. Biophys. Res. Commun. 94*, 600−605.
68. Davis, J. C., and Averill, B. A. (1982) *Proc. Natl. Acad. Sci. U.S.A. 79*, 4623−4627.
69. Beck, J. L., Keough, D. T., de Jersey, J., and Zerner, B. (1984) *Biochim. Biophys. Acta 791*, 357−363.
70. Beck, J. L., McArthur, M. J., de Jersey, J., and Zerner, B. (1988) *Inorg. Chim. Acta 153*, 39−44.
71. David, S. S., and Que, L., Jr. (1990) *J. Am. Chem. Soc. 112*, 6455−6463.
72. Holz, R. C., Que, L., Jr., and Ming, L.-J. (1992) *J. Am. Chem. Soc. 114*, 4434−4436.
73. Suerbaum, H., Körner, M., Witzel, H., Althaus, E., Mosel, B.-D., and Müller-Warmuth, W. (1993) *Eur. J. Biochem. 214*, 313−321.
74. Merkx, M., and Averill, B. A. (1998) *Biochemistry 37*, 8490−8497.

BI982606U